

Electronic Supporting Information

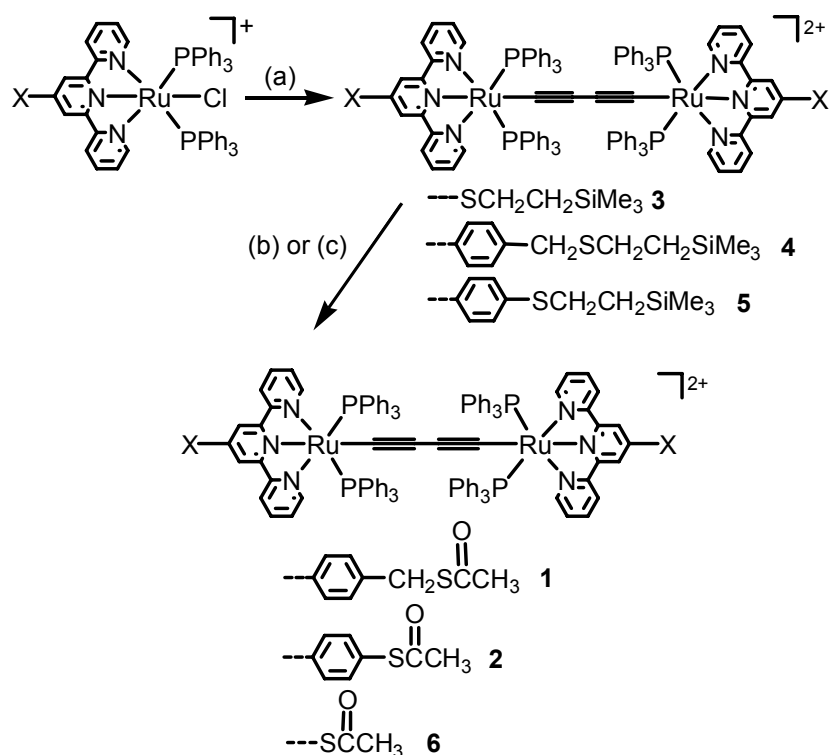
Electrical Conductance Study on 1,3-Butadiyne-linked Dinuclear Ruthenium(II) Complexes within Single Molecule Break Junctions

Hui-Min Wen,^a Yang Yang,^b Xiao-Shun Zhou,^c Jun-Yang Liu,^b Dao-Bin Zhang,^a Zhao-Bin Chen,^b Jin-Yun Wang,^a Zhong-Ning Chen,*^a and Zhong-Qun Tian*^b

^a State Key Laboratory of Structural Chemistry, Fujian Institute of Research on the Structure of Matter, Chinese Academy of Sciences, Fuzhou, Fujian 350002, China.

^b State Key Laboratory of Physical Chemistry of Solid Surfaces and Department of Chemistry, College of Chemistry and Chemical Engineering, Xiamen University, Xiamen, Fujian 361005, China.

^c Zhejiang Key Laboratory for Reactive Chemistry on Solid Surfaces, Institute of Physical Chemistry, Zhejiang Normal University, Jinhua, Zhejiang 321004, China



Scheme S1. Synthetic routes for thiol-functionalized diruthenium compounds **1-6**. (a) 1,4-bis(trimethylsilyl)-1,3-butadiyne, TEA, CH₃OH, microwave irradiation, 100 °C. (b) AgClO₄, acetyl chloride, CH₃CN, r. t. (c) TBAF, acetyl chloride, THF, r. t.

As shown in Scheme S1, a series of TMSE-protected (TMSE = 2-(trimethylsilyl)ethyl) sulphur-functionalized dinuclear ruthenium(II) complexes linked by 1,3-butadiyne were successfully prepared in a one-pot process under microwave irradiation. TMSE-protective thiol-functionalized complexes **4** and **5** could be readily converted into corresponding acetyl-protected counterparts **1** and **2**, which are more favourable for molecular self-assembly in conductance measurement although corresponding acetyl-protected complex **6** (Scheme S1) was inaccessible by this approach. Nevertheless, the protective group TMSE in **3** could be readily removed in the presence of fluoride so that conductance measurement was directly performed without conversion to **6**. The ¹H NMR spectral studies (Fig. S1) indicated that **3** could be suitable for conductance measurement through fluoride-promoted desiliconizing reaction (Fig. S2) at ambient temperature.

Thiol-functionalized dinuclear ruthenium(II) complexes (Scheme 1) were characterized by ESI-MS spectrometry, ¹H and ³¹P NMR, and UV-Vis spectroscopy,

and electrochemistry. The UV-Vis spectra of these dinuclear ruthenium(II) complexes in CH₃CN displayed intense absorption bands in the UV region due to ligand-centred transitions together with a broad band at ca. 630 nm arising from dπ(Ru)→π*(tpy) MLCT transition (Fig. S3). Cyclic voltammetric studies on **1–3** in 0.1 M TBAP-CH₂Cl₂ solutions revealed three reversible redox waves (Fig. S4) at ca. 0.32, 0.84 and 1.41 V vs. the Ag/AgCl, ascribed to stepwise one-electron processes Ru₂^{II,II}/Ru₂^{III,II}, Ru₂^{III,II}/Ru₂^{III,III}, and Ru₂^{III,III}/Ru₂^{III,IV}, respectively. The potential difference ($\Delta E_{1/2} = 0.52$ V) between the first and second redox waves was comparable to that of other 1,3-butadiyne linked diruthenium analogues,^{13,14} suggesting that a quite large Ru…Ru electronic interaction is transmitted across bridging 1,3-butadiyne. It appears that subtle difference in peripheral terpyridine ligands exerts inappreciable influence on the redox properties of **1–3**.

Experimental Section

Materials and Reagents

All synthetic operations were carried out under dry argon atmosphere by using Schlenk techniques at ambient temperature and vacuum-line system unless specified. The solvents were dried, distilled and degassed prior to use, except those for spectroscopic measurements were of spectroscopic grade. The reagents 1,4-bis(trimethylsilyl)-1,3-butadiyne (Me₃SiC≡CC≡CSiMe₃), acetyl chloride, silver perchlorate (AgClO₄), tertabutylammonium fluoride (TBAF), and tertabutylammonium perchlorate (TBAP) were purchased from commercial sources (Alfa Aesar, Acros and Aldrich Chemical Co.). [(TMSESCH₂C₆H₄tpy)(PPh₃)₂RuCl](ClO₄), [(TMSESC₆H₄tpy)(PPh₃)₂RuCl](ClO₄), and [(TMSEStpy)(PPh₃)₂RuCl](ClO₄) were synthesized as previously described procedures.¹ The microwave irradiation synthesis was performed by Biotage Initiator system.

Caution! Perchlorate salts are potentially explosive and should be handled carefully in a small amount.

Synthesis of **4**.

To a microwave vial (30 mL) were added

[(TMSESC₆H₄tpy)(PPh₃)₂RuCl](ClO₄) (300 mg, 0.25 mmol) and 1,4-bis(trimethylsilyl)-1,3-butadiyne (Me₃SiC≡CC≡CSiMe₃) (29.1 mg, 0.15 mmol) under argon atmosphere. The vessel was charged with triethylamine (NEt₃) (5 mL) and methanol (15 mL), and sealed quickly with a microwave tube cap. Under microwave radiation, the mixture was heated in 100 °C for 30 min. Upon cooling to room temperature, the reaction mixture was poured into another flask and evaporated *in vacuo*. The product was purified by column chromatograph on a silica gel using dichloromethane-acetone (10:1) as eluent to collect green band, giving green solid product. Yield: 56% (167 mg). IR (KBr, cm⁻¹): $\tilde{\nu}$ = 1993 (w, C≡C), 1247 (w, Si—C), 1089 (s, ClO₄), 697 (s, P—C). ESI-MS: m/z (%) = 1105 (100) [M - (ClO₄)₂]²⁺. ¹H NMR (CD₃CN, ppm): δ = 0.06 (s, 18H), 0.94 (m, 4H), 2.58 (m, 4H), 3.89 (s, 4H), 6.90 (t, J = 7.5 Hz, 24H), 7.10 (t, J = 7.4 Hz, 12H), 7.14 (t, J = 6.4 Hz, 4H), 7.58–7.71 (m, 32H), 7.74 (m, 8H), 7.90 (d, J = 8.0 Hz, 4H), 9.00 (d, J = 5.4 Hz, 4H). ³¹P NMR (CD₃CN, ppm): δ = 25.97 (s). Anal. Calcd. for C₁₃₀H₁₁₈Cl₂N₆O₈P₄Ru₂S₂Si₂: C, 64.80; H, 4.94; N, 3.49. Found: C, 64.65; H, 4.75; N 3.56.

Synthesis of 5

This compound was prepared by the same procedure as that of **4** except using [(TMSESC₆H₄tpy)(PPh₃)₂RuCl](ClO₄) instead of [(TMSESC₆H₄tpy)(PPh₃)₂RuCl](ClO₄). Yield: 54%. IR (KBr, cm⁻¹): $\tilde{\nu}$ = 1990 (w, C≡C), 1248 (w, Si—C), 1089 (s, ClO₄), 697 (s, P—C). ESI-MS: m/z (%) = 1091 (100) [M - (ClO₄)₂]²⁺. ¹H NMR (CD₃CN, ppm): δ = 0.13 (s, 18H), 1.04 (m, 4H), 3.17 (m, 4H), 6.90 (s, J = 7.5 Hz, 24H), 7.07–7.16 (m, 16H), 7.52–7.75 (m, 40H), 7.90 (d, J = 8.0 Hz, 4H), 9.00 (d, J = 5.3 Hz, 4H). ³¹P NMR (CD₃CN, ppm): δ = 25.97 (s). Anal. Calcd. for C₁₂₈H₁₁₄Cl₂N₆O₈P₄Ru₂S₂Si₂: C, 64.55; H, 4.82; N, 3.53. Found: C, 64.13; H, 4.76; N, 3.67.

Synthesis of 3

This compound was prepared by the same procedure as that of **4** except using [(TMSEStpy)(PPh₃)₂RuCl](ClO₄) instead of [(TMSESC₆H₄tpy)(PPh₃)₂RuCl](ClO₄). Yield: 60%. IR (KBr, cm⁻¹): $\tilde{\nu}$ = 1993 (w, C≡C), 1247 (w, Si—C), 1089 (s, ClO₄), 697 (s, P—C). ESI-MS: m/z (%) = 1015 (100) [M - (ClO₄)₂]²⁺. ¹H NMR (CD₃CN, ppm): δ = 0.21 (s, 18H), 1.10 (m, 4H), 3.21 (m,

4H), 6.91 (t, $J = 7.6$ Hz, 24H), 7.11 (m, 16H), 7.34 (s, 4H), 7.59–7.67 (m, 28H), 7.75 (d, $J = 7.8$ Hz, 4H), 8.94 (d, $J = 5.5$ Hz, 4H). ^{31}P NMR (CD_3CN , ppm): $\delta = 26.14$ (s). Anal. Calcd. for $\text{C}_{116}\text{H}_{106}\text{Cl}_2\text{N}_6\text{O}_8\text{P}_4\text{Ru}_2\text{S}_2\text{Si}_2\cdot\text{H}_2\text{O}$: C, 61.99; H, 4.84; N, 3.74. Found: C, 62.03; H, 4.65; N, 3.64.

Synthesis of 1

A mixture of silver perchlorate (5 equiv.) and excess acetyl chloride (10 equiv.) was stirred vigorously in dry CH_3CN at room temperature in darkness. When silver chloride precipitated completely, TMSE-protected thioether **4** was added to the solution with stirring for 30 min. The mixture was filtered and to the filtrate was added a saturated aqueous solution of NaHCO_3 which was extracted with dichloromethane. The combined organic layers were dried in Na_2SO_4 and the solvent removed *in vacuo*. The residue was chromatographed on a silica gel column using dichloromethane-acetone (10:1) as eluent. Yield: 85%. IR (KBr, cm^{-1}): $\tilde{\nu} = 1997$ (w, $\text{C}\equiv\text{C}$), 1684 (m, $\text{C}=\text{O}$), 1089 (s, ClO_4), 696 (s, P–C). ESI-MS: m/z (%) = 760 (100) $[(\text{AcSCH}_2\text{C}_6\text{H}_4\text{tpy})(\text{PPh}_3)_2\text{Ru}]^+$, 1047 (10) $[\text{M} - (\text{ClO}_4)_2]^{2+}$. ^1H NMR (CD_3CN , ppm): $\delta = 2.41$ (s, 6H), 4.27 (s, 4H), 6.90 (t, $J = 7.5$ Hz, 22H), 7.07–7.16 (m, 16H), 7.58–7.74 (m, 42H), 7.89 (d, $J = 8.0$ Hz, 4H), 9.00 (d, $J = 5.5$ Hz, 4H). ^{31}P NMR (CD_3CN , ppm): $\delta = 25.93$ (s). Anal. Calcd. for $\text{C}_{124}\text{H}_{98}\text{Cl}_2\text{N}_6\text{O}_{10}\text{P}_4\text{Ru}_2\text{S}_2$: C, 64.95; H, 4.31; N, 3.66. Found C, 64.78; H, 4.20; N, 3.47.

Synthesis of 2

To a solution of the TMSE-protected compound **5** in dry THF was added 10 equiv. THF solution of TBAF (1.0 M). The reaction mixture was stirred at room temperature for 1 h, followed by the addition of 20 equiv. acetyl chloride. Upon completion, the solution was diluted with dichloromethane and a saturated aqueous solution of NaHCO_3 , and then washed with water for three times. The collected organic layers were dried in Na_2SO_4 and the solvent removed *in vacuo*. The acetylthio-functionalized product was purified by chromatography on a silica gel column using dichloromethane-acetone (10:1) as eluent. Yield: 88%. IR (KBr, cm^{-1}): $\tilde{\nu} = 1997$ (w, $\text{C}\equiv\text{C}$), 1698 (m, $\text{C}=\text{O}$), 1090 (s, ClO_4), 697 (s, P–C). ESI-MS: m/z (%) = 1033 (10) $[\text{M} - (\text{ClO}_4)_2]^{2+}$, 747 (100) $[(\text{AcSC}_6\text{H}_4\text{tpy})(\text{PPh}_3)_2\text{Ru}]^+$. ^1H NMR (CD_3CN , ppm): $\delta = 2.51$ (s, 6H), 6.91 (t, $J = 7.6$ Hz, 24H), 7.10 (t, $J = 7.4$ Hz, 12H), 7.16 (t, $J = 7.4$ Hz, 12H).

6.1 Hz, 4H), 7.63–7.71 (m, 32H), 7.79 (s, 4H), 7.85 (d, J = 8.1 Hz, 4H), 7.91 (d, J = 8.1 Hz, 4H), 9.01 (d, J = 5.4 Hz, 4H). ^{31}P NMR (CD_3CN , ppm): δ = 25.77 (s). Anal. Calcd. for $\text{C}_{122}\text{H}_{94}\text{Cl}_2\text{N}_6\text{O}_{10}\text{P}_4\text{Ru}_2\text{S}_2$: C, 64.69; H, 4.18; N, 3.71. Found: C, 64.75; H, 4.32; N, 3.64.

The Desilication Reaction of TMSE-protected Diruthenium Complex **3** with TBAF

Within a few minutes upon mixing the fluoride ion source (TBAF) with compound **3** in $\text{THF}-d_8$, the proton signal of SiMe_3 disappeared completely (Fig. S1a). Meanwhile, a new single peak (δ = 5.36 ppm) occurred as shown in Fig. S1b, which is the characteristic chemical shift of ethylene ($\text{CH}_2=\text{CH}_2$) protons in $\text{THF}-d_8$. Furthermore, ethylene can be removed in vacuum, which was demonstrated in Fig. S1c. The ^1H NMR spectral studies thus indicated that the reaction of **3** with TBAF was indeed conducted with formation of ethylene.

Preparation of Self-Assembled Monolayer (SAM) and Surface Electrochemical Measurements

An Au(111) electrode was immersed into a EtOH solution of **1** or **2** (1.0 mM) for 1 d. It was taken out and rinsed thoroughly with EtOH and dried in an argon atmosphere. The gold electrode modified with the monolayer of **1** or **2** was used as a working electrode for cyclic voltammetry measurements in a 0.1 M NaClO_4 aqueous solution. Platinum wire and saturated calomel electrode (SCE) were used as the counter and reference electrodes, respectively.

Conductance Measurements

A homebuilt electrochemically assisted-mechanically controllable break junction (EC-MCBJ) setup was used to measure the single molecule conductance of dinuclear ruthenium complexes. First, a stepping motor was turned up to bend the microchip and elongate the connected electrode pair, during which the conductance was monitored. At a certain displacement of the stepping motor, the conductance dropped to 1 G_0 , corresponding to a single Au atom bridged two electrodes. Then the stepping motor was turned up further to break this single atom bridge to get a nanometer-sized gap. Second, the gap width was maintained at 3–4 nm, and 3–5 droplets of the measured molecules were placed over surfaces of Au electrodes pair. Since these

molecules are likely to contact Au surfaces, as indicated in our electrochemical studies, a diluted THF solution of 0.1 mM and an insufficient assembly time of 10 min were adopted. It was assumed that an uncompact SAM layer would be formed under such assembly condition, leaving some diffusion degree for the molecules attached onto the Au electrode pair. Then a 100 mV bias was applied in order to make the measured molecules align along the electrode pair, and improve the Au-molecule-Au junction formation probability during the subsequent conductance measurements. Since TMSE-protected diruthenium complex **3** was sensitive to fluoride ion of TBAF (Fig. S1 and S2), fabrication of Au-**3**-Au molecular junctions was performed after mixing **3** with TBAF in a THF solution. Third, the molecular conductance measurements were carried out with 20 mV of bias during breaking and re-establishing the electrode pair repeatedly, and several hundreds of conductance traces with discernable plateaus were obtained and used to construct conductance histograms. All the experiments were carried out under ambient conditions.

Physical Measurements

UV-Vis absorption spectra were measured on a Perkin-Elmer Lambda 25 UV-Vis spectrophotometer. Infrared spectra (IR) were recorded on a Magna 750 FT-IR spectrophotometer with KBr pellets. Elemental analyses (C, H, N) were carried out on a Perkin-Elmer model 240 C elemental analyzer. Electrospray ionization mass spectrometry (ESI-MS) was performed on a Finnigan LCQ mass spectrometer using dichloromethane-methanol mixtures as mobile phases. The cyclic voltammograms (CVs) were made with a potentiostat/galvanostat model 263A in dichloromethane solution containing 0.1 M *n*-Bu₄NClO₄ (TBAP) as the supporting electrolyte. The CVs were performed at a scan rate of 100 mV s⁻¹. Platinum and glassy graphite were used as the counter and working electrodes, respectively, and the potential was measured against an Ag/AgCl (saturated KCl) reference electrode.

Quantum Chemistry Computation

The geometrical optimizations were performed with Gaussian 03 program package^{2,3} at the B3PW91 level (Becke's three-parameter hybrid functional/Perdew and Wang correlation functional).⁴ The initial structures were extracted as isolated molecules derived from the experimentally determined geometry obtained from the

X-ray crystallographic data. To save the computation time, the reduced models were used, in which all the phenyl groups in triphenylphosphine (PPh_3) were replaced by H atoms. In the optimization process, the convergent values of maximum force, root-mean-square (RMS) force, maximum displacement, and RMS displacement are set by default. In these calculations, the Lanl2dz⁵ effective core potential (ECP) was employed to describe the inner electrons of ruthenium(II) atoms, and the associated double- ζ basis set was used for the remaining outer electrons. To precisely describe the electron character, one additional f-type polarization function was added for ruthenium ($\alpha_f = 1.235$)⁶ atoms. The other nonmetal atoms were described by 6-311G** all-electron basis set.

The electronic structures and transport properties of the extended molecules were investigated by using the TRANSIENT method,⁷⁻⁹ which involved the solution of the electronic density from the DFT Hamiltonian using Green's functions. The system was divided into three parts: the left electrode, the scattering region, and the right electrode. The gold electrodes were grown along the (111) direction. The electrode calculations were performed with three layers of gold and 100 k-points along the transport direction (z). The scattering region includes the extended molecule and four gold layers as the buffer layer along the transport direction on each side of the molecule, which ensures a smooth transition between the surface and the bulk of the gold electrodes. Au–S bond distance at both ends is about 0.21 nm in the hollow-hollow (H-H) configuration in order to ensure the same bonding geometry, thus avoiding the possible bonding site effects on the considered transmission, as depicted in Fig. S10 for **3**.^{10,11}

We used a single-zeta (SZ) basis set for the gold and a double-zeta polarized (DZP) basis set for the molecule. The Hamiltonian and the overlap matrix elements were calculated within an energy cutoff of 200 Ry. The local density approximation (LDA) was employed to calculate the exchange and correlation energy, and the occupation of the electronic states were determined by Fermi-Dirac occupation function with a temperature of 100 K.

References

1. H.-M. Wen, D.-B. Zhang, L.-Y. Zhang, L.-X. Shi and Z.-N. Chen, *Eur. J. Inorg. Chem.*, 2011, **11**, 1784.
2. (a) P. Hohenberg and W. Kohn, *Phys. Rev.*, 1964, **136**, B864; (b) W. Kohn and L. J. Sham, *Phys. Rev.*, 1965, **140**, A1133.
3. M. J. Frisch, G. W. Trucks, H. B. Schlegel, G. E. Scuseria, M. A. Robb, J. R. Cheeseman, J. A. Montgomery, Jr., T. Vreven, K. N. Kudin, J. C. Burant, J. M. Millam, S. S. Iyengar, J. Tomasi, V. Barone, B. Mennucci, M. Cossi, G. Scalmani, N. Rega, G. A. Petersson, H. Nakatsuji, M. Hada, M. Ehara, K. Toyota, R. Fukuda, J. Hasegawa, M. Ishida, T. Nakajima, Y. Honda, O. Kitao, H. Nakai, M. Klene, X. Li, J. E. Knox, H. P. Hratchian, J. B. Cross, V. Bakken, C. Adamo, J. Jaramillo, R. Gomperts, R. E. Stratmann, O. Yazyev, A. J. Austin, R. Cammi, C. Pomelli, J. W. Ochterski, P. Y. Ayala, K. Morokuma, G. A. Voth, P. Salvador, J. J. Dannenberg, V. G. Zakrzewski, S. Dapprich, A. D. Daniels, M. C. Strain, O. Farkas, D. K. Malick, A. D. Rabuck, K. Raghavachari, J. B. Foresman, J. V. Ortiz, Q. Cui, A. G. Baboul, S. Clifford, J. Cioslowski, B. B. Stefanov, G. Liu, A. Liashenko, P. Piskorz, I. Komaromi, R. L. Martin, D. J. Fox, T. Keith, M. A. Al-Laham, C. Y. Peng, A. Nanayakkara, M. Challacombe, P. M. W. Gill, B. Johnson, W. Chen, M. W. Wong, C. Gonzalez and J. A. Pople, Gaussian 03, revision D.02. Gaussian, Inc.: Wallingford, CT, 2004.
4. (a) A. D. Becke, *Phys. Rev. A*, 1988, **38**, 3098; (b) J. P. Perdew and Y. Wang, *Phys. Rev. B*, 1992, **45**, 13244.
5. (a) P. J. Hay and W. R. Wadt, *J. Chem. Phys.*, 1985, **82**, 270; (b) W. R. Wadt and P. J. Hay, *J. Chem. Phys.*, 1985, **82**, 284; (c) P. J. Hay and W. R. Wadt, *J. Chem. Phys.*, 1985, **82**, 299.
6. A. W. Ehlers, M. Böhme, S. Dapprich, A. Gobbi, A. Höllwarth, V. Jonas, K. F. Köhler, R. Stegmann, A. Veldkamp and G. Frenking, *Chem. Phys. Lett.*, 1993, **208**, 111.
7. J. M. Soler, E. Artacho, J. D. Gale, A. García, J. Junquera, P. Ordejón, and D. Sanchez-Portal, *J. Phys.: Condens. Matter*, 2002, **14**, 2745.
8. M. Brandbyge, J.-L. Mozos, P. Ordejón, J. Taylor and K. Stokbro, *Phys. Rev. B*, 2002, **65**, 165401.
9. J. P. Perdew and A. Zunger, *Phys. Rev. B*, 1981, **23**, 5048.

10. V. Kaliginedi, P. Moreno-García, H. Valkenier, W. Hong, V. M. García-Suárez, P. Buiter, J. L. H. Otten, J. C. Hummelen, C. J. Lambert and T. Wandlowski, *J. Am. Chem. Soc.*, **2012**, 134, 5262.
11. Ž. Crljen and G. Baranović, *Phys. Rev. Lett.*, **2007**, 98, 116801.

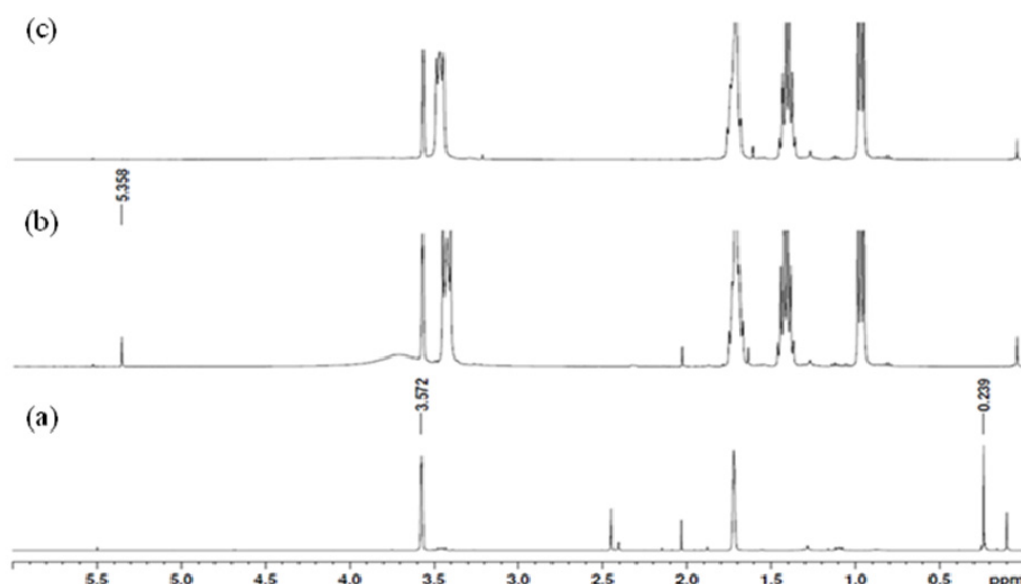


Fig. S1. ^1H NMR spectra of the desiliconizing reaction of (a) **3**, (b) **3** and TBAF, (c) after vacuuming treatment of (b) and reprogramming in $\text{THF}-d_8$.

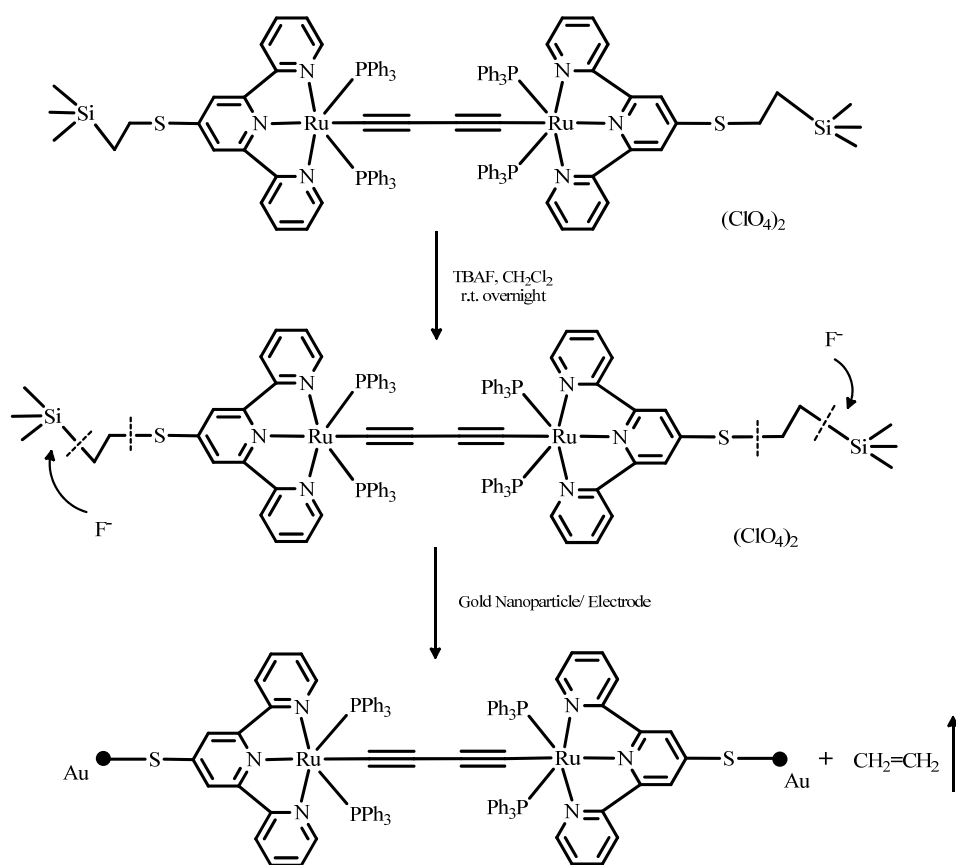


Fig. S2. Concrete routes for the reaction of TMSE-protected diruthenium complex **3** and TBAF, and the formation of Au-S bond.

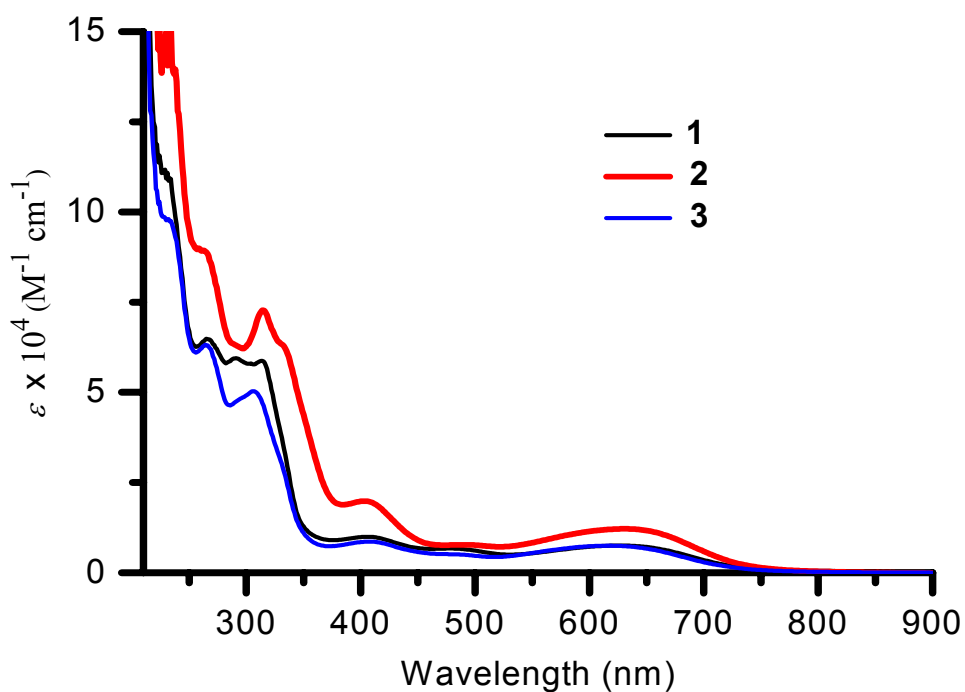


Fig. S3. UV-Vis spectra of **1** (black line), **2** (red line), and **3** (blue line).

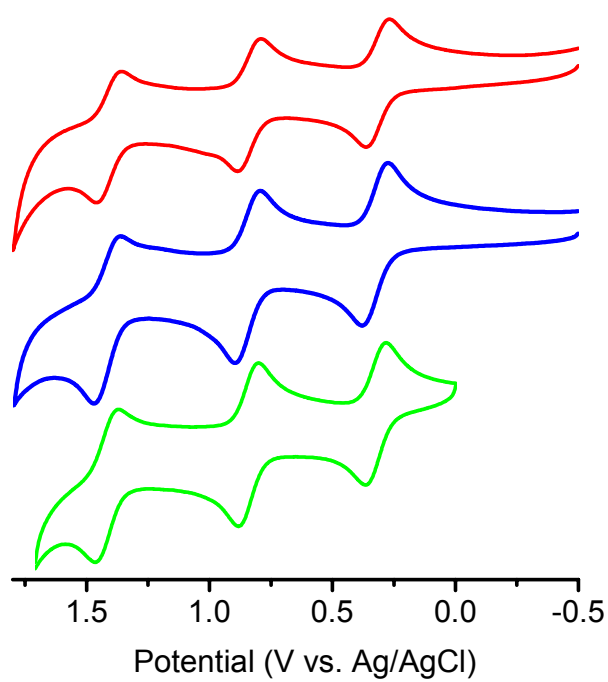


Fig. S4. Plots of cyclic voltammograms of **1** (red line), **2** (blue line), and **3** (green line) in a 0.1 M TBAP-CH₂Cl₂ solution. The scan rate is 100 mV s⁻¹.

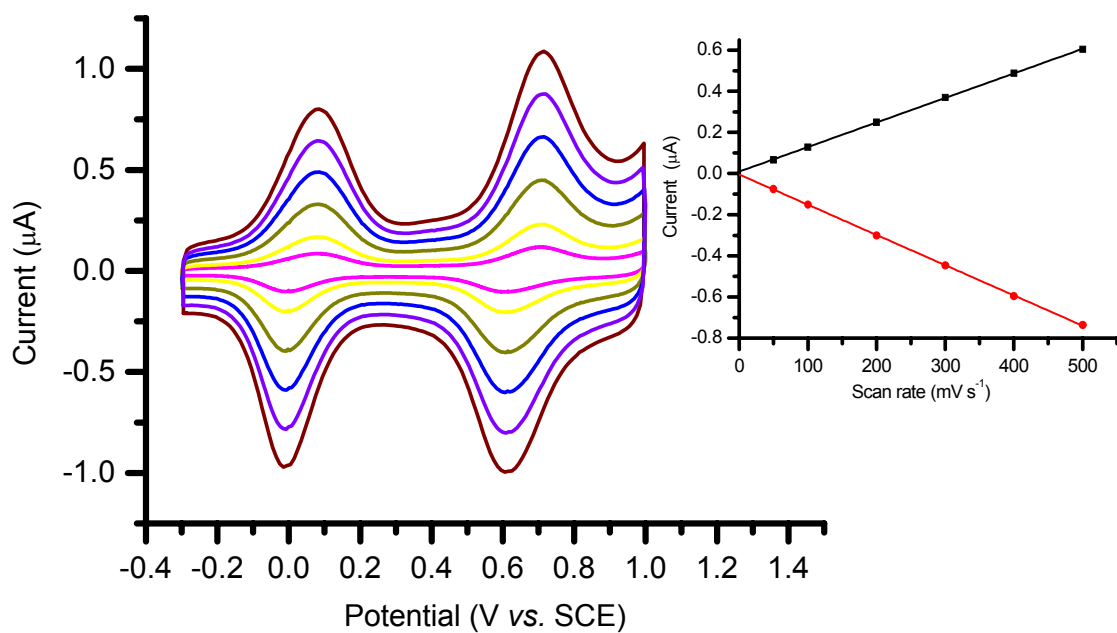


Fig. S5. Cyclic voltammograms (CVs) of self-assembled films of **2** on single crystal Au(111) electrode surfaces in a 0.1 M NaClO₄ aqueous solution. The scan rates are 50, 100, 200, 300, 400, and 500 mV s⁻¹, respectively. Inset: linear dependence of the peak currents as a function of scan rate.

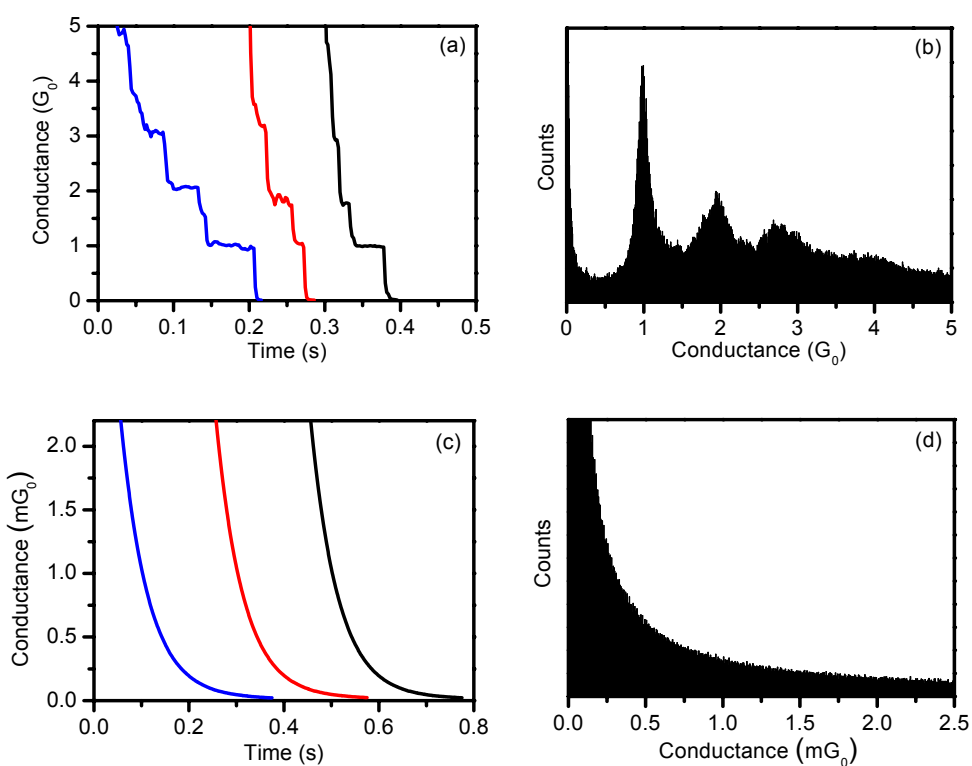


Fig. S6. Typical conductance traces and the corresponding histogram recorded in our MCBJ setup without target molecules. (a) Conductance traces of the contact region. (b) Histogram of the contact region. (c) Conductance traces of the tunneling current region, (d) Histogram of the tunneling current region.

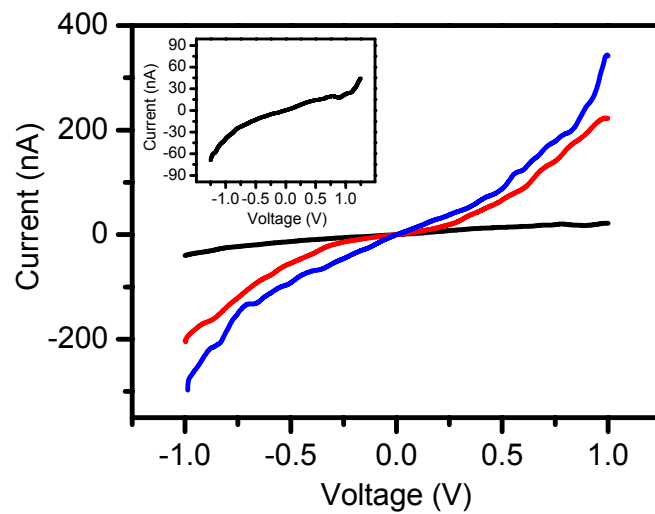


Fig. S7. Representative $I-V_{\text{bias}}$ curves measured for a molecular junction constructed by **1** (black), **2** (red), or **3** (blue), respectively with the MCBJ setup. Inset: the representative $I-V_{\text{bias}}$ curve of an Au-**1**-Au junction was magnified for clarity.

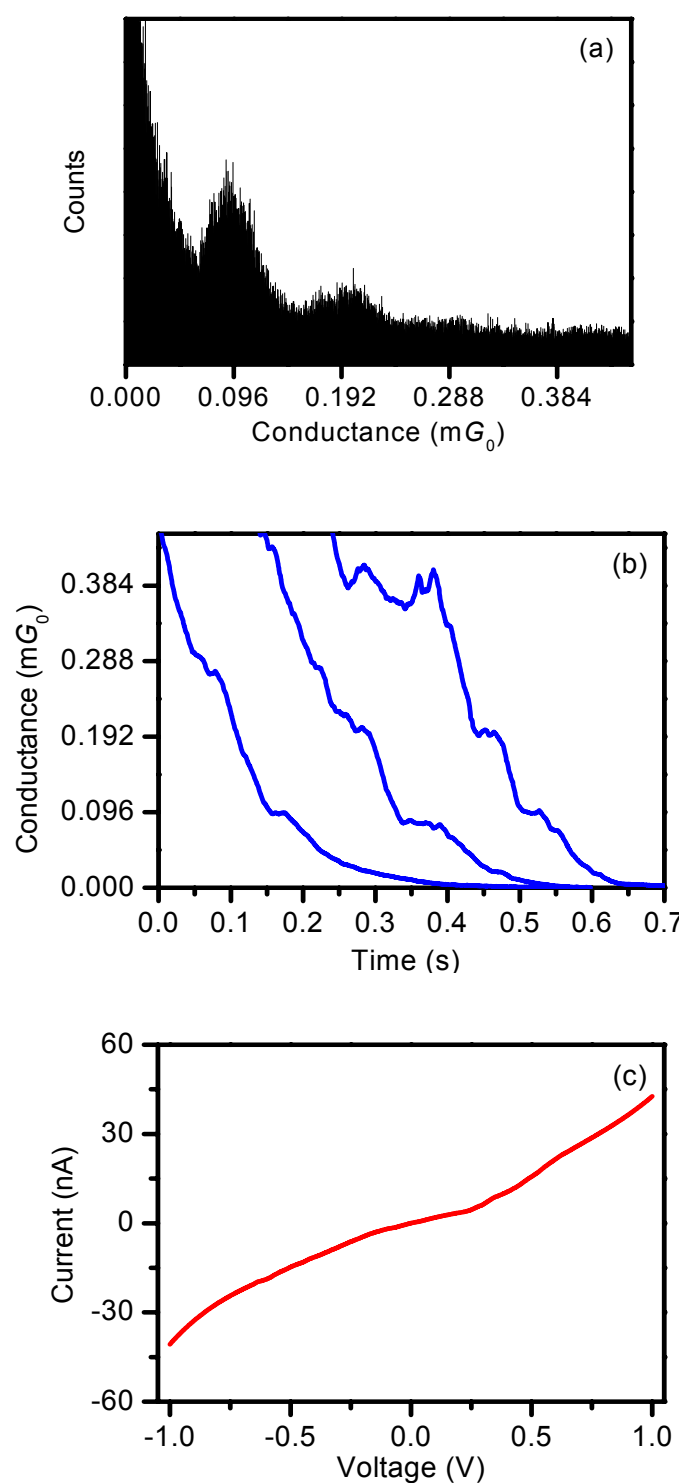


Fig. S8. (a) Conductance histogram of OPE from hundreds of curves recorded in the MCBJ setup.
(b) Typical conductance traces of the OPE molecule. (c) Representative $I-V_{\text{bias}}$ curve measured for a molecular junction constructed by OPE molecule with the MCBJ setup.

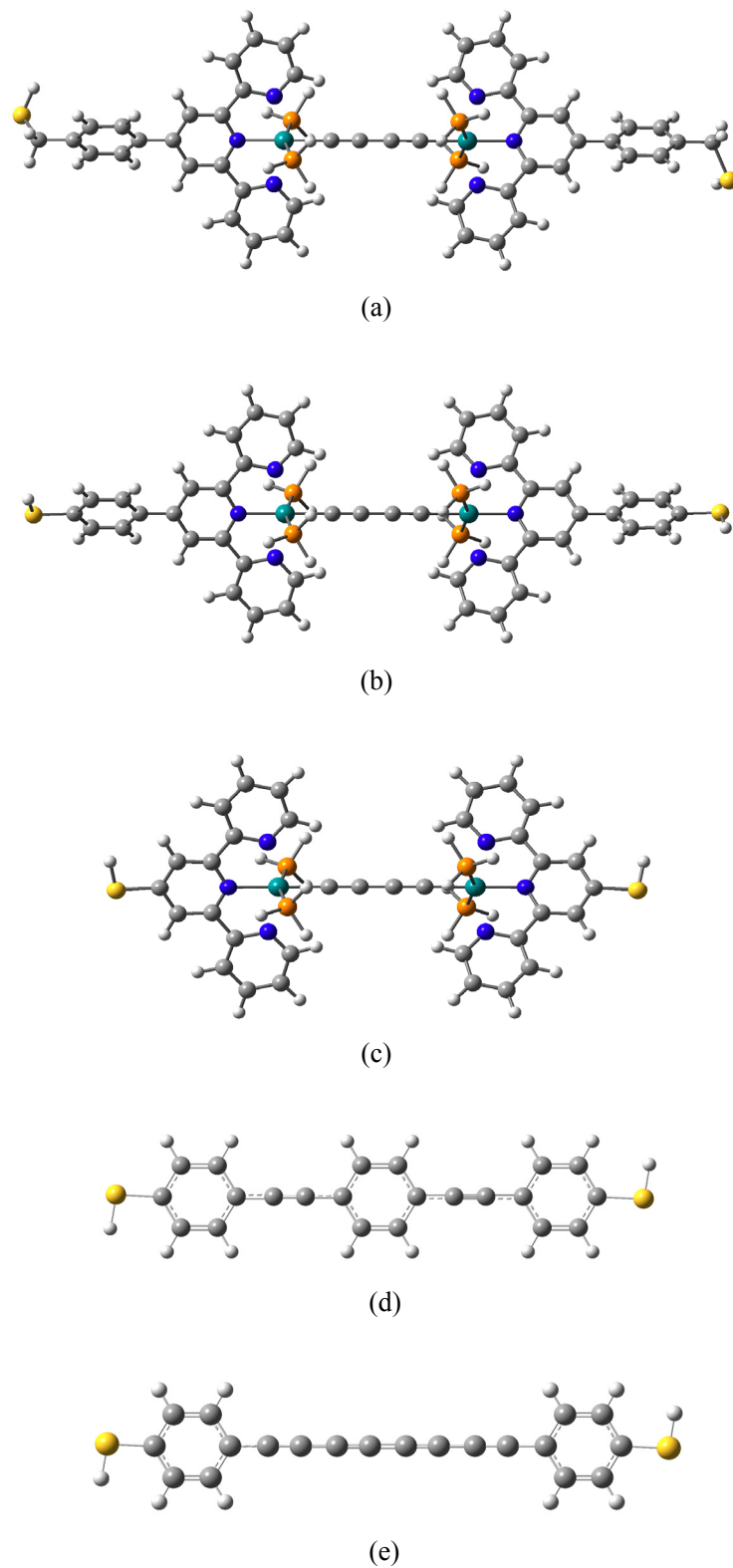


Fig. S9. The optimized geometrical structures of (a) **1**, (b) **2**, (c) **3**, (d) OPE3, and (e) DPA4 at B3PW91/ 6-311G**/Lanl2dz(*f*) level, in which all the phenyl groups in triphenylphosphine (PPh₃) were replaced by H atoms. The distances of intramolecular S···S atoms are 3.06, 2.96, 2.09, 2.01, and 2.09 nm, respectively.

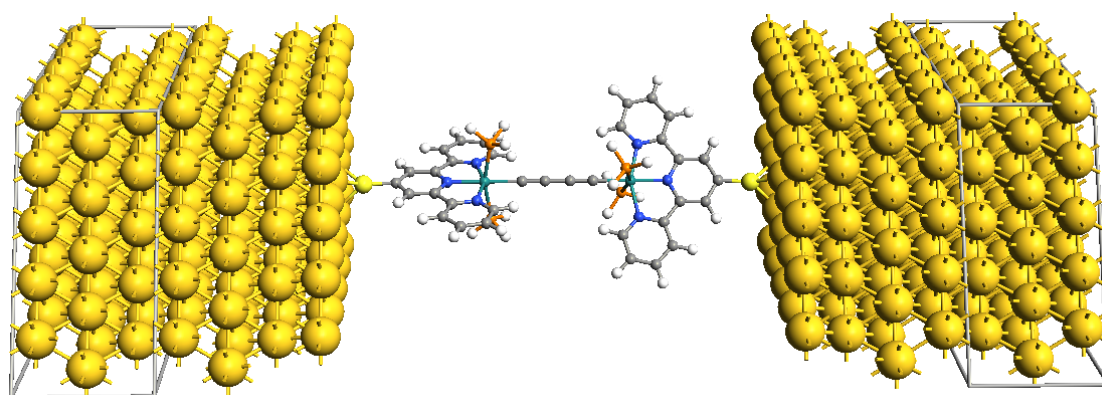


Fig. S10. Schematic representation of the extended molecule used in the calculations, corresponding to the optimized geometrical structure of **3**, which was coupled in the hollow-hollow (H-H) configuration. The grey square frames represent the unit cells of bulk gold grown along (111) direction.

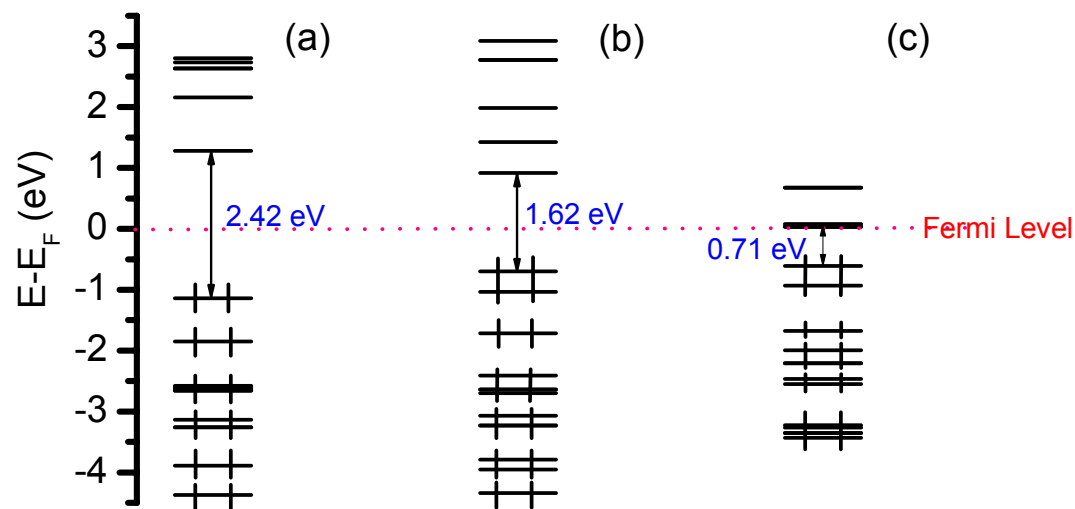


Fig. S11. The energy levels of frontier molecular orbitals of (a) OPE3, (b) DPA4, and (c) **3**.

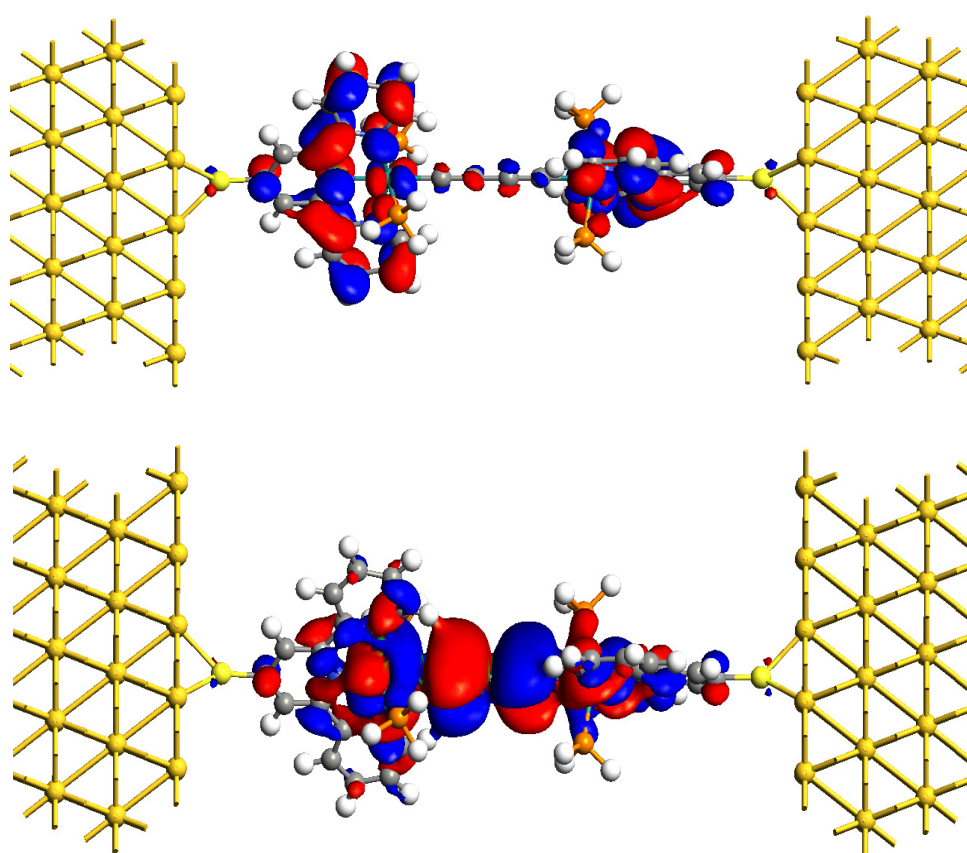


Fig. S12. The diagrams of MPSH LUMO (upper) and HOMO (lower) of complex **3** connected to two Au(111) surface via Au–S bonds.